Supporting Information for:

Solvothermal Synthesis of ZnO-Decorated α-Fe_2O_3 Nanorods with Highly Enhanced Gas-Sensing Performance toward n-Butanol

Yusuf V. Kaneti[a], Quadir M.D. Zakaria[a], Zhengjie Zhang[a], Chuyang Chen[a], Jeffrey Yue[b], Minsu Liu[a], Xuchuan Jiang[a,*] and Aibing Yu[a]

[a]*School of Materials Science and Engineering, The University of New South Wales, Sydney NSW 2052, Australia*

[b]*Department of Chemical Engineering, University College London, Torrington Place, London WC1E 7JE, United Kingdom.*

1. Gas-sensing measurement system diagram

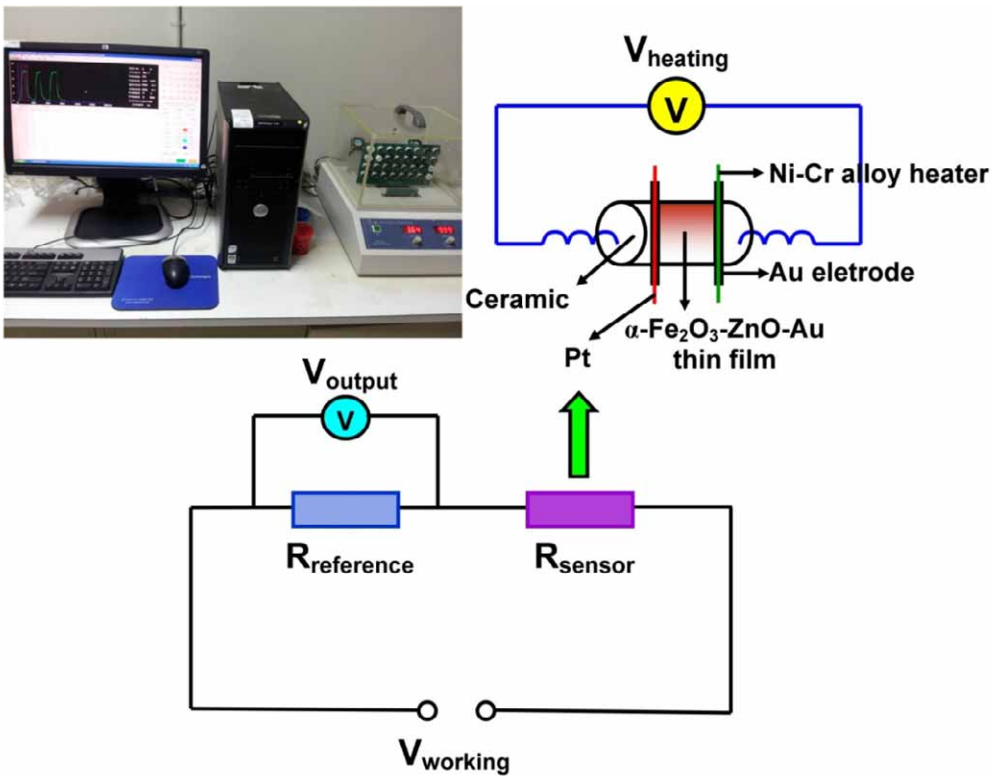

Fig. S1 Schematic diagram of the gas-sensing measurement system.

[*] To whom correspondence should be addressed. Email: xcjiang@unsw.edu.au.

2. Digital photographs of the sensors

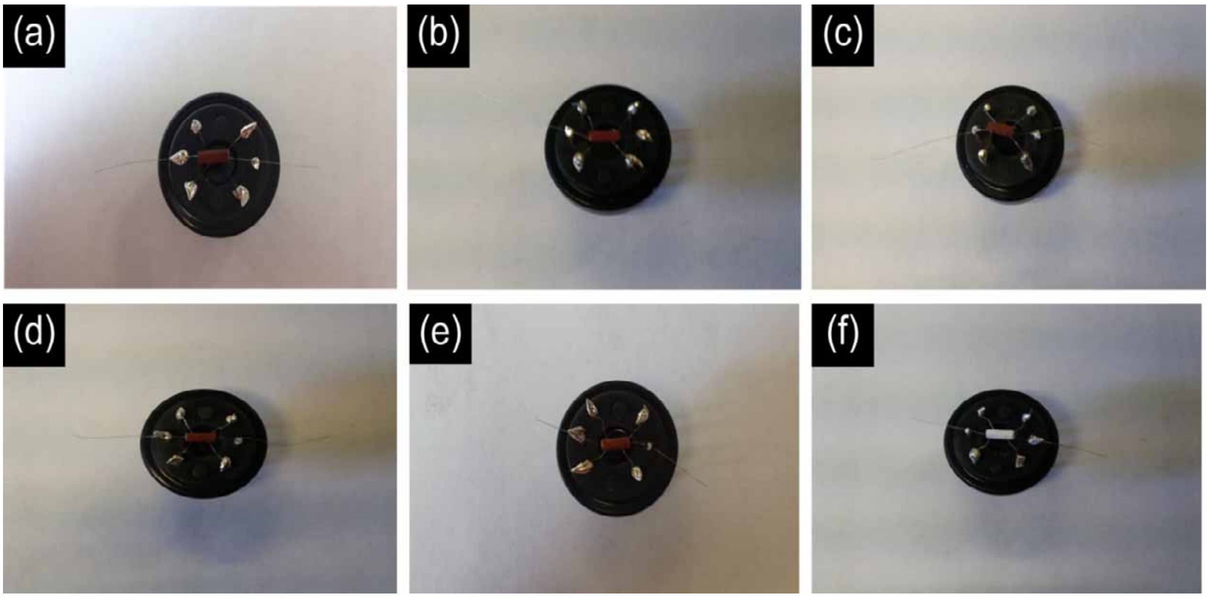

Fig. S2 Digital photographs of the prepared sensors: (a) α-Fe_2O_3 nanorods, (b) α-Fe_2O_3/ZnO (S1), (c) α-Fe_2O_3/ZnO (S2), (d) α-Fe_2O_3/ZnO (S3), (e) α-Fe_2O_3/ZnO (S4), and (f) ZnO nanorods.

3. SEM images of α-Fe_2O_3 nanorods, ZnO decorated α-Fe_2O_3 nanorods, and ZnO nanorods

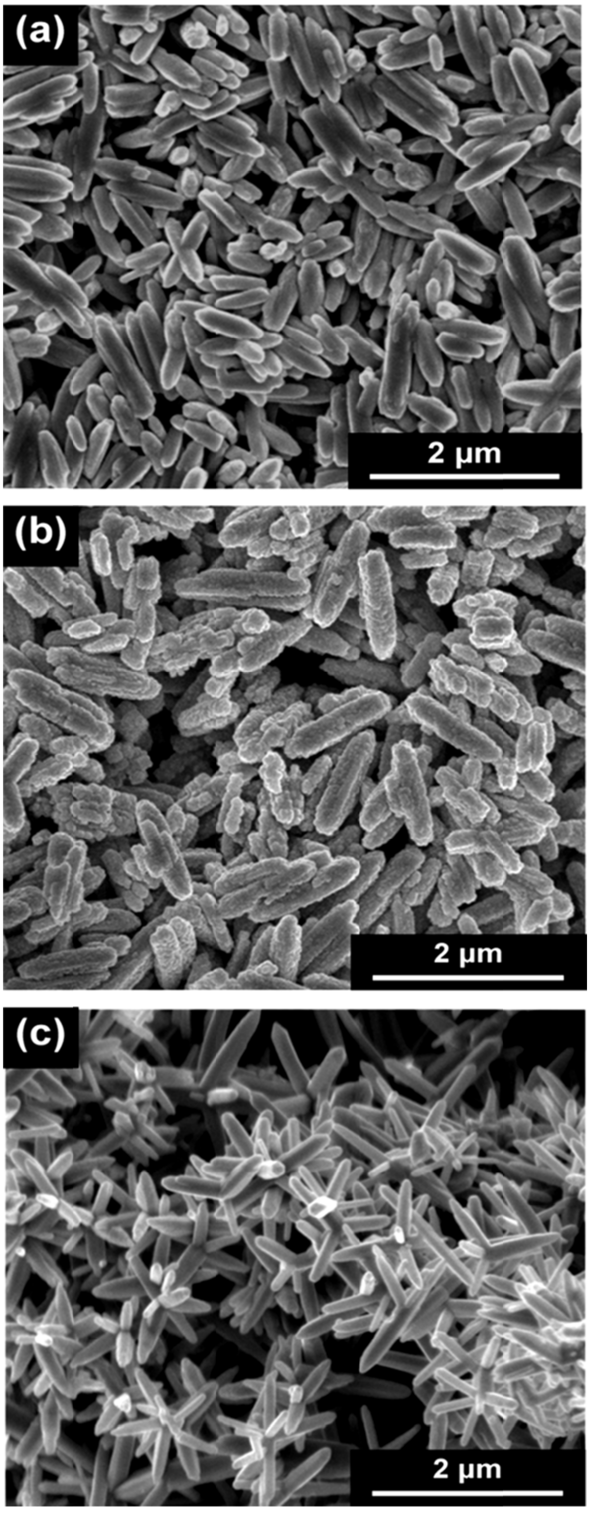

Fig. S3 SEM images of: (a) α-Fe_2O_3 nanorods, (b) ZnO decorated α-Fe_2O_3 nanorods, and (c) ZnO nanorods.

4. Effect of Zinc Precursor - TEM images

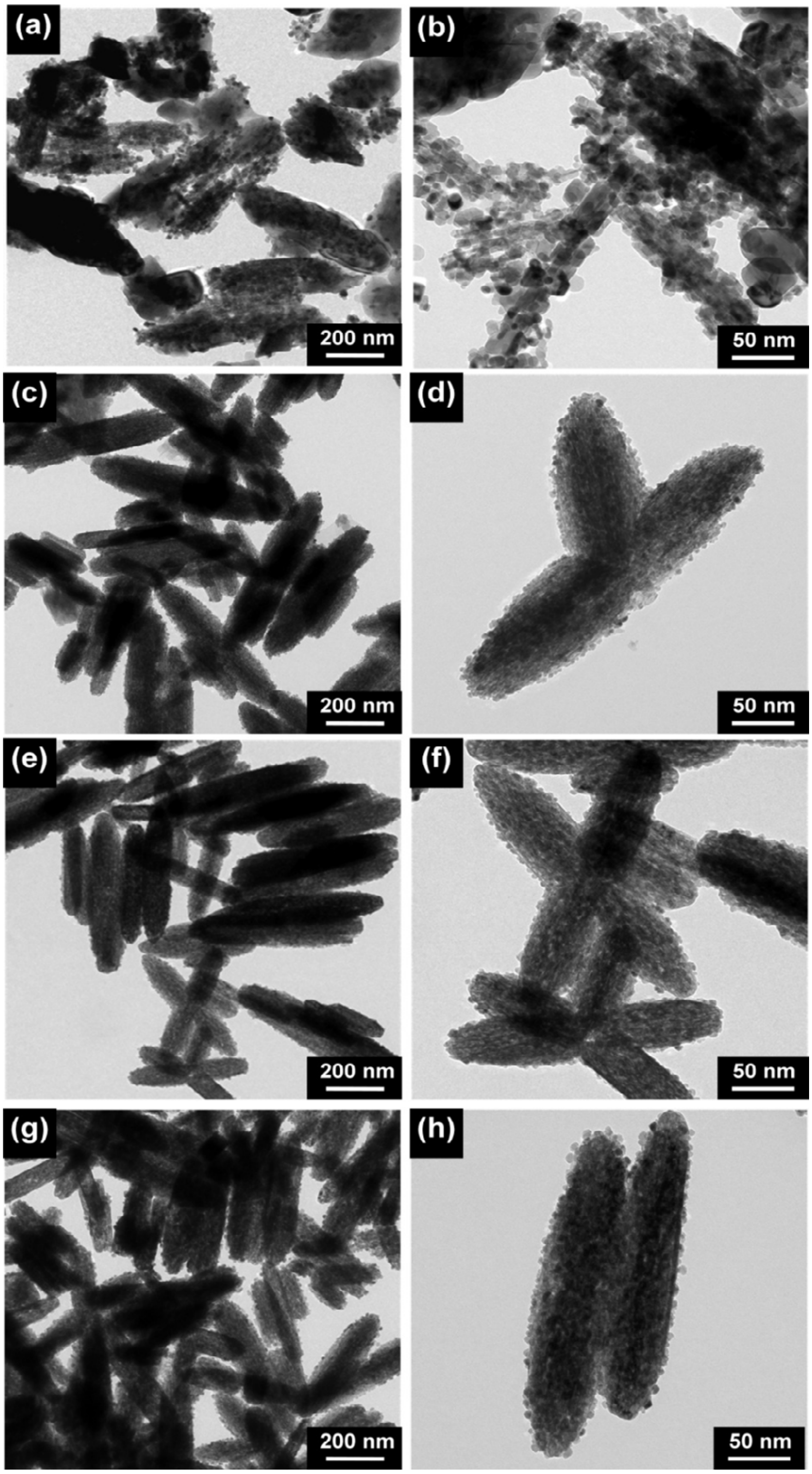

Fig. S4 TEM images of α-Fe_2O_3/ZnO products obtained with different amounts of Zn precursor ($ZnSO_4.7H_2O$): (a, b) 0.0036 g (S1), (c, d) 0.018 g (S2), (e. f) 0.0269 g (S3), and (g, h) 0.0359 g (S4).

5. BET Surface Area and pore-size distribution

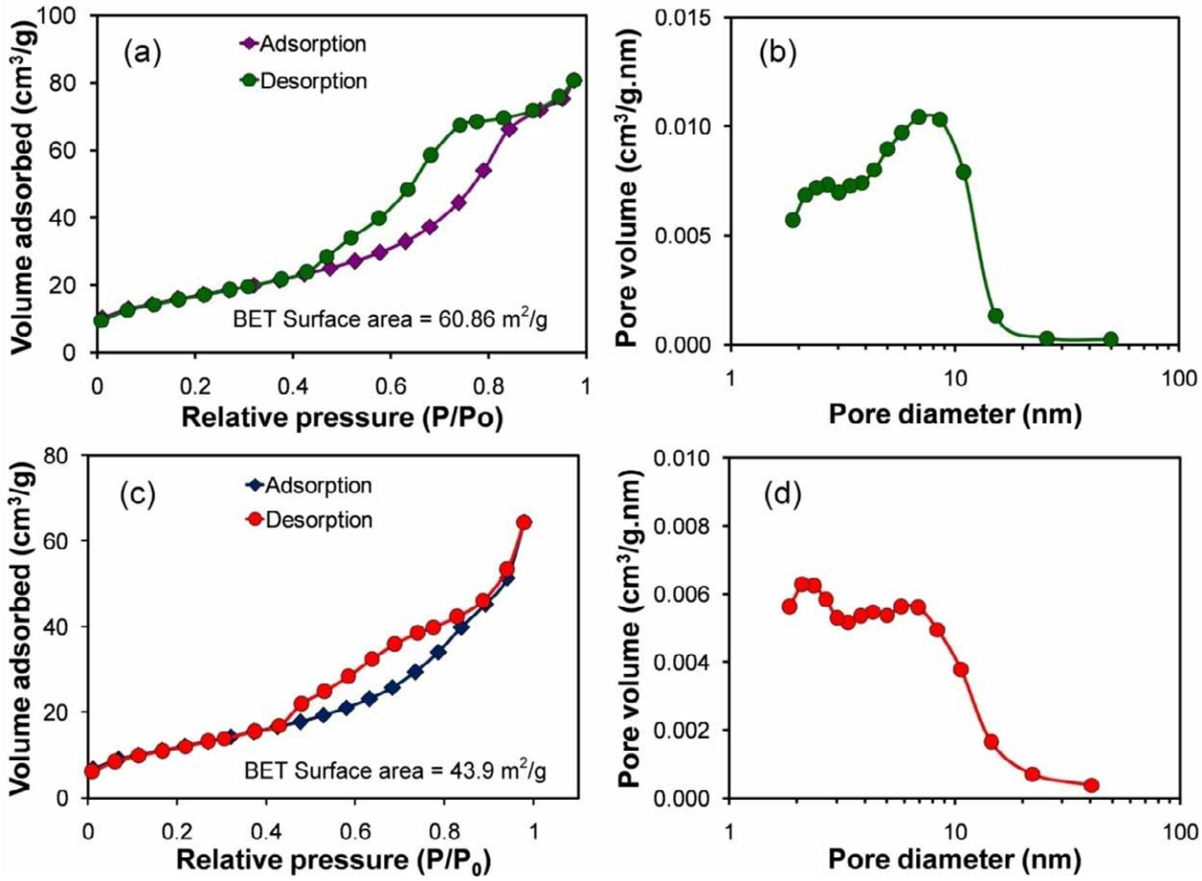

Fig. S5 The N_2 adsorption-desorption isotherms and pore size distribution plots of: (a, b) pure α-Fe_2O_3 nanorods and (b) ZnO decorated α-Fe_2O_3 nanorods (S4).

Fig. S5a and b show the N_2 adsorption-desorption isotherms and Barret-Joyner-Halenda (BJH) pore size distribution plot of the porous α-Fe_2O_3 nanorods. Based on the IUPAC classification, the isotherm can be ascribed to a type IV isotherm with a type H1 hysteresis loop in the P/P_0 range of ~0.4-0.9. The BJH distribution plot shown in Figure S5b shows the presence of a primary pore size distribution peak centered at ~2.5 nm and a secondary distribution peak centered at 8 nm. These results indicate the mesoporous nature of the as-prepared α-Fe_2O_3 nanorods. The BET surface area of the as-synthesized α-Fe_2O_3 nanorods is measured to be 60.86 m^2/g. In comparison, The BET surface area of the ZnO-decorated α-Fe_2O_3 nanorods (sample S4) is slightly lower (~44 m^2/g), because of the slight increase in the sizes of the α-Fe_2O_3 nanorods during the ZnO coating process in the autoclave (at 180 °C). The BJH distribution plot of the ZnO-decorated α-Fe_2O_3 nanorods shown in Figure S5d shows the presence of a primary pore size distribution peak centered at ~2.2 nm and a secondary distribution peak centered at ~7 nm. Similar to the pure α-Fe_2O_3 nanorods, the isotherm of the ZnO-decorated α-Fe_2O_3 nanorods can also be indexed to a type IV isotherm with a type H3 hysteresis loop in the P/P_0 range of ~0.4-0.95. The BJH pore distribution plot of the ZnO-decorated α-Fe_2O_3 nanorods depicted in Figure S5d reveals the existence of a primary pore size distribution peak centered at ~2.2 nm and a secondary distribution peak centered at ~7 nm, which confirms their mesoporous nature.

6. Dynamic response-recovery curves toward methanol, ethanol, and acetone

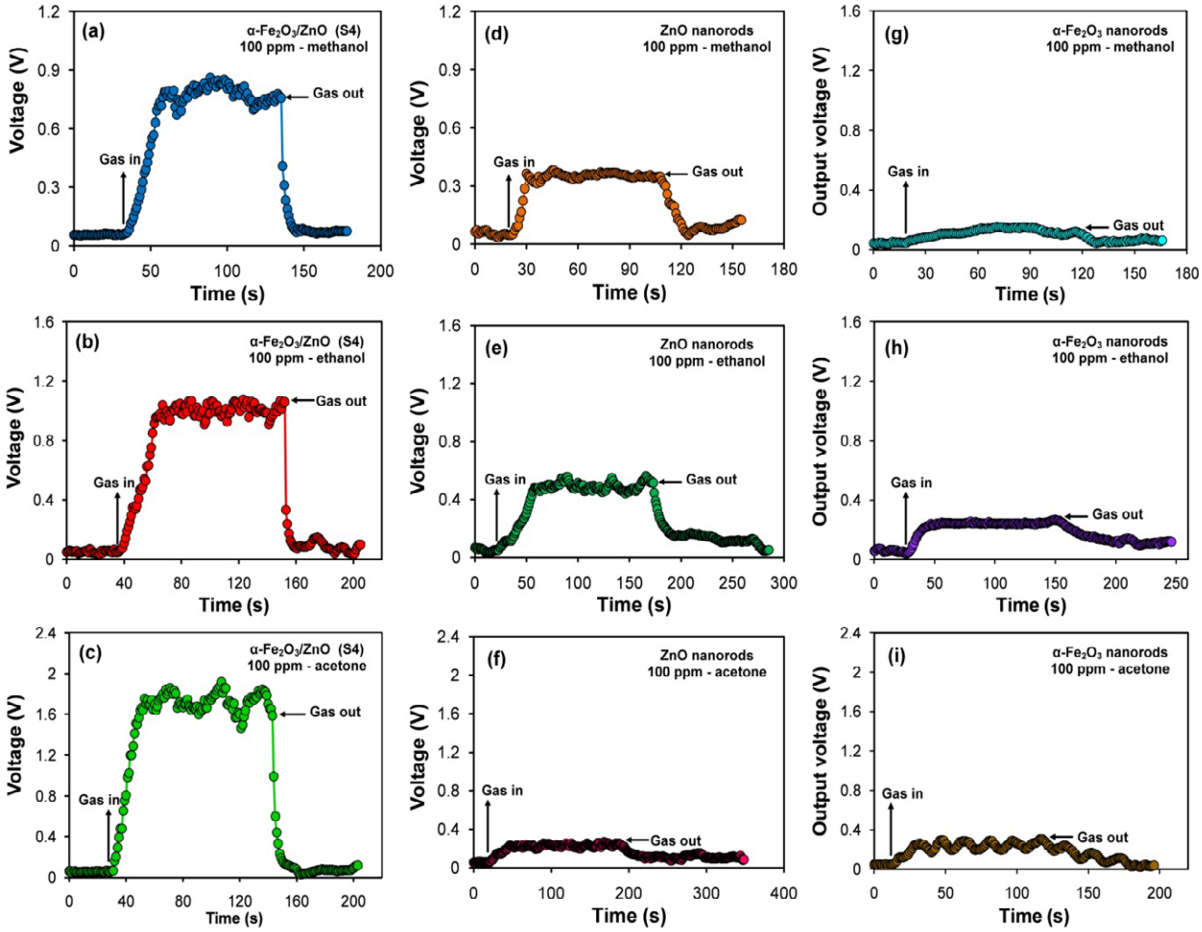

Fig. S6 Dynamic response-recovery curves of ZnO-decorated α-Fe_2O_3 nanorods (S4) toward 100 ppm of (a) methanol, (b) ethanol, and (c) acetone; Dynamic response-recovery curves of ZnO nanorods toward 100 ppm of (d) methanol, (e) ethanol, and (c) acetone; Dynamic response-recovery curves of α-Fe_2O_3 nanorods toward 100 ppm of (g) methanol, (h) ethanol, and (i) acetone.

7. Additional gas-sensing experiments- ZnO nanoparticles

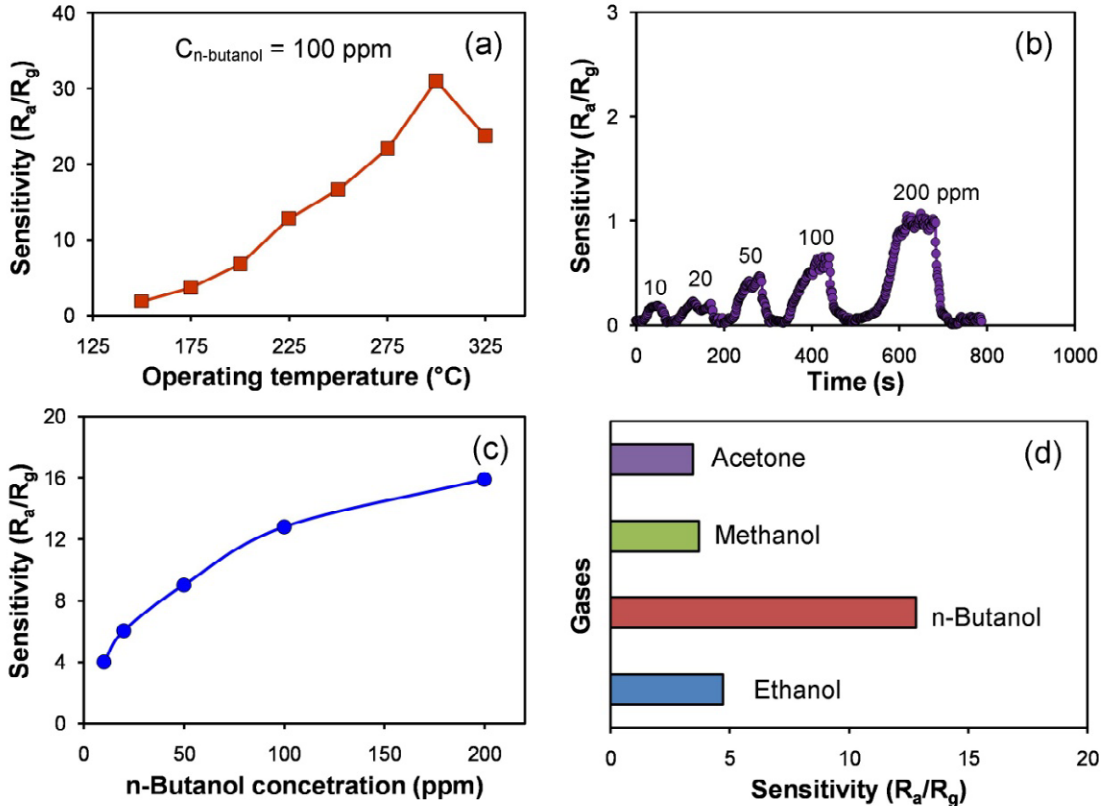

Fig. S7 The sensitivity of the sensor based on ZnO nanoparticles toward 100 ppm of n-butanol as a function of the operating temperature, (b) dynamic response-recovery behaviors of the ZnO nanoparticle sensor toward various concentrations of n-butanol at the optimum working temperature of 225 °C, (c) the sensitivity *vs*. concentration curves of the ZnO nanoparticle sensor toward *n*-butanol at 225 °C, and (d) selectivity tests of the ZnO nanoparticle sensor toward various VOCs at 225 °C.

Additional gas-sensing tests have been performed for ZnO nanoparticles prepared by the same procedure used for decorating the α-Fe_2O_3 nanorods as shown in Fig. S7. The results show that the sensor based on ZnO nanoparticles exhibits the maximum sensitivity toward n-butanol at a higher optimum operating temperature of 300 °C. The concentration dependent test show that the ZnO nanoparticles exhibit a sensitivity of S = 12.8 toward 100 ppm of n-butanol at 225 °C, which is approximately 4.5 times lower than the ZnO-decorated α-Fe_2O_3

nanorods and is comparable to the gas-sensing properties of pure α-Fe_2O_3 nanorods. This suggests that synergistic effects, arising from the combination of the two materials, may have been responsible for the enhanced performance of the α-Fe_2O_3/ZnO nanocomposites.